Structural Characterization of MacroH2A Containing Chromatin†

D. Wade Abbott,‡ Mario Laszczak,‡ John D. Lewis,‡ Harvey Su,‡,§ Susan C. Moore,‡,|| Melissa Hills,‡,+ Stefan Dimitrov,# and Juan Ausió*,‡

Department of Biochemistry and Microbiology, University of Victoria, Victoria, British Columbia, Canada, V8W 3P6, Department of Zoology, University of British Columbia, British Columbia, Canada, V6T 1Z4, The Prostate Center, Vancouver General Hospital, British Columbia, Canada, V6H 3Z6, Department of Biology, University of Victoria, Victoria, British Columbia, Canada, V8W 3P6, and Laboratoire d'Etudes de la Différenciation et de l'Adhérence Cellulaires, UMR CNRS/UJF 5538, Institut Albert Bonniot, 38076 La Trouche Cedex, France

Received October 15, 2003; Revised Manuscript Received November 24, 2003

ABSTRACT: MacroH2A (mH2A) is one of the most recently identified members of the heteromorphous histone variant family. It is unique among the members of this group because it contains an unusually large non-histone C-terminal end, from where its name derives, and appears to be restricted to subphylum vertebrata. Although a concerted effort has been carried out in order to characterize the physiological relevance of mH2A, little is known in comparison about the structural importance of the molecule. Elucidating the biophysical and conformational proprieties of mH2A in chromatin may provide clues into the links between this histone variant and its unique function(s). In this paper, we look first at the heterogeneous tissue-specific distribution of this protein in different vertebrate classes. This is followed by a structural comparison between mH2A and H2A protein and by the characterization of the nucleosome core particles with which these histone subtypes are associated. We find that the highly α-helical C-terminus of mH2A confers an asymmetric conformation to nucleosomes and that this variant is tightly bound to chromatin fragments in a way that does not depend on the overall extent of acetylation of the other core histones.

Within the nucleus, DNA is associated with histone and non-histone proteins to form a highly dynamic nucleoprotein complex called chromatin. This assembly is characterized by the repetitive organization of well-defined histone−DNA complexes referred to as nucleosomes. The nucleosome core particle is a bipartite structure, consisting of a octameric protein core complete with two molecules each of histone H2A, H2B, H3, and H4, that constrains 146 bp of DNA in approximately one and three-quarter left-handed supercoils around its perimeter (see ref *1* for the crystal structure of the nucleosome core particle). Upon association with linker histones, nucleosome arrays fold into a chromatin fiber that hinders the DNA potential for activation events such as transcription (*2*, *3*) and repair (*4*−*6*). Although this organization may present a thermodynamic obstacle to both processive and distributive enzymatic complexes, accumulating experimental evidence provides strong support for the active involvement of histones in the regulation of gene expression. Examples of these epigenetic events include histone post-translational modifications and histone variant exchange. The downstream effects of such histone variability coordinates the structural transitions required for the regulation of gene expression in either a combinatorial fashion, which generates a histone code that is interpreted by trans-acting factors (*7*, *8*) or by directly affecting the conformation of the chromatin fiber (*9*, *10*).

Currently, the roles of histone variants in chromatin structure and function are the object of an extensive biochemical and biophysical characterization (see refs *9* and *10*). Histone variants are nonallelic isoforms that replace major histones within specialized chromatin domains. In humans, the genes of these subtypes are absent from the canonic histone gene cluster and are expressed outside of the of S phase of the cell cycle (*11*, *12*). This suggests that the functions of these gene products are not exclusive to the structural packaging of newly replicated DNA and are important for constitutive regulatory events. Histone variants can be classified based on the heterogeneity of their primary structure, which is ultimately responsible for the structural variability of the specialized chromatin domains with which these variant histones are associated. This can be achieved by altering either the structural or informational nature of such regions (*9*, *10*).

One such histone variant, macroH2A (mH2A),[1] is unique in that it displays an extensive non-histone fusion at its carboxyl end. This non-histone region (NHR), which constitutes two-thirds of the molecular mass of the protein, contains a short basic region and a putative leucine zipper domain. mH2A copurifies with native mononucleosomes (*13*,

† This work was supported by a Canadian Institutes of Health Research (CIHR) MOP-57718 grant to J.A. and INSERM to S.D. W.D.A. was a recipient of a National Sciences and Engineering Research Council (NSERC) doctorate PGS B fellowship.

* To whom all correspondence should be addressed. Phone: (250) 721-8863. Fax: (250) 721-8855. E-mail: jausio@uvic.ca.

‡ Department of Biochemistry and Microbiology, University of Victoria.

§ University of British Columbia.

|| Vancouver General Hospital.

+ Department of Biology, University of Victoria.

Institut Albert Bonniot.

[1] Abbreviations: LB, Luria-Bertani; MCB, macrochromatin body; mH2A, macroH2A; NHR, non-histone region; SOPM, self-optimized protein method; TCA, trichloroacetic acid.

10.1021/bi035859i CCC: $27.50 © 2004 American Chemical Society
Published on Web 01/13/2004

14) and can be reconstituted into nucleosomes in vitro (*15*, *16*). In vivo, mH2A is expressed as two nonallelic gene products: mH2A1 (which is posttranscriptionally spliced to generate two minor subtypes mH2A1.1 and mH2A1.2) and mH2A2. Although distinct functions have yet to be ascribed to mH2A1 and mH2A2, temporal expression differences have been observed between the mH2A1 isoforms. Whereas mH2A1.1 seems to accumulate during development and differentiation, mH2A1.2 appears to remain constant (*17*).

Cytologically, mH2A has been shown to coalesce into a structure called a macrochromatin body (MCB), which is coincident with the inactivated X-chromosome (*18*−*20*) and the XY-body of spermatocytes (*21*, *22*). Although mH2A has been coupled to sex-linked heterochromatinization, specialized nucleosomes containing this variant must be required for further nuclear functions, as expression levels appear highest in liver tissue (*17*) and are equivalent in both male and female somatocytes (*14*, *23*). It is possible that mH2A may be dynamically involved in the global regulation of tissue specific and developmental transcription. In vitro assays have shown that the NHR of the molecule represses expression of the luciferase reporter gene in Gal4 fusion experiments (*24*). Further interactions of this histone variant with the heterochromatin protein M31 (*25*) and its colocalization with methylated H3−K4 during metaphase at a potential activation boundary (*14*) provide additional support to this notion.

In an attempt to further elucidate the role of mH2A in chromatin function, we have explored the structural properties of mH2A containing nucleosomes. Our findings indicate that mH2A mononucleosomes are quite asymmetric, likely due to the extensions of the distinctive carboxyl tails of the mH2A molecule, and exhibit a stability that is very similar to that of native nonvariant nucleosome core particles. Interestingly, mH2A exhibits an enhanced binding affinity for chromatin than that exhibited by H2A. Indeed, this binding affinity appears to be independent of the extent of core histone acetylation.

MATERIALS AND METHODS

Acid Extraction of Histones. Nuclei were isolated from different tissues and organisms as described for chicken erythrocytes (*26*). Hydrochloric acid extracted histones were then obtained from these nuclei as described in ref *27*.

Western Blotting. Western blots were performed following hydroxyapatite fractionation and acid extraction of animal histones. mH2A1 was detected with a primary rabbit polyclonal antibody raised against the nonhistone portion (*18*). Approximately 2 μg of histones was loaded onto SDS−polyacrylamide gels and transferred to a PVDF membrane at 100 V for 2.5 h at 4 °C in 25 mM Tris-HCl (pH 7.5) and 192 mM glycine. The membrane was prepared by dipping into 100% methanol for 5 s followed by rinses in dH_2O and transfer buffer. Blotted membranes were blocked in PBS (*28*), 0.1% Tween, 3% skimmed milk overnight at 4 °C. mH2A antibodies were used at a 1:3500 (30 mL) dilution with shaking for 1.5 h at room temperature in PBS, 0.1% Tween, 350 mM NaCl, followed by four 15 min washes with PBS and 0.1% Tween. The membrane was then incubated with secondary anti-rabbit horseradish peroxidase antibody (NEN, Boston, MA) for 45 min at a 1:3000 dilution (30 mL). Following this, the blot was extensively washed four times for 15 min with PBS and 0.1% Tween followed by four 10 min washes with PBS and rinsed with distilled water. Visualization of the protein bands was carried out according to the manufacturer's instructions (NEN, Boston, MA).

Expression and Purification of Recombinant mH2A1.2. Recombinant mH2A1.2 was expressed and purified as according to ref *15*. Briefly, *Escherichia coli* BL21(DE3) expression cells were transformed with a pGEX-4T-1 (Amersham Biotech, Cleveland, OH) mH2A1.2 construct that contains an N-terminal GST fusion (kindly provided by J. R. Pehrson). Transformants were cloned and used to inoculate 300 mL of Luria−Bertani (LB) broth containing 50 μg/mL ampicillin, which was then incubated with vigorous shaking at 22.5 °C for 2 days. This culture was added to 1.2 L of fresh LB and incubated under the same conditions for 1 h. Protein expression was induced with 0.1 mM IPTG. Cells were harvested after 3 h by centrifugation. mH2A1.2 was affinity purified from sonicated and clarified lysate using glutathione Sepharose 4B beads (Amersham Pharmacia Biotech). This was followed by Macroprep High S ionic exchange (Bio-Rad, Randolph, MA) chromatography with a 0.5−2.0 M NaCl gradient in 10 mM Tris (7.5), 1 mM DTT, 0.2 mM PMSF. Finally, fractions containing mH2A1.2 were pooled, loaded onto a hydroxyapatite column, and eluted by a 0−100 mM $NaPO_4$ gradient in 1.0 M NaCl, 10 mM Tris (7.5), 1 mM DTT, 0.2 mM PMSF. Appreciable amounts of mH2A1.2 as determined by SDS gels were combined and used directly for reconstitution experiments.

Circular Dichroism. Circular dichroism (CD) spectra for mH2A1.2 were determined at 20 °C on a Jasco- J720 spectropolarimeter as previously described (*29*). The amount of α-helix was quantified as described in ref *30*.

Secondary Structure Prediction. The α-helical content of rat mH2A1.2 (ascension number AAB38330) and chicken H2A (ascension number HSCH2A) was predicted by the SOPM (self-optimized protein method) method (*31*) located on the ExPasy Proteomics server (http://ca.expasy.org/tools/#secondary). mH2A1.2 and H2A profiles were aligned schematically to compare relative distributions of secondary structure between the two proteins (*31*).

Reconstitution of mH2A1.2 Nucleosomes. Recombinant mH2A1.2 was expressed and purified as described above (*15*). Chicken erythrocyte native H2B, H3, and H4 core histones were prepared as described in Abbott et al. (*32*). Core histones were mixed at a ratio of 9:1:1:1 (mH2A/H2B/H3/H4) as estimated by SDS−polyacrylamide gel electrophoresis (*33*). This excess of mH2A1.2 was required to generate reconstituted particles with slower electrophoretic mobility, which was determined to contain the proper stoichiometry of core histones following SDS−PAGE analysis. In some instances, mH2A containing complexes of higher electrophoretic mobility (similar to that of native chicken erythrocyte) could be clearly visualized, which were determined to be depleted in one mH2A−H2B dimer as determined by sucrose gradient purification (results not shown). The protein mixture was combined with 146 bp DNA at a ratio of (1.5:1.0) to bring the final DNA concentration to approximately 100 μg DNA/mL in 2 M NaCl, 10 mM Tris-HCl (pH 7.5), 10 mM β-mercaptoethanol, 0.1 mM EDTA. Reconstitutions were performed by decreasing the sodium chloride concentration from 2 to 0 M by stepwise salt

gradient dialysis as in ref *34* in the same buffer. Reconstituted particles were analyzed by electrophoresis in 4% native acrylamide as described in ref *35*.

DNAse I and Hydroxyl Radical Footprinting. For the DNase I footprinting, 10 ng of DNase I was used to digest 10 μL of the reconstituted nucleosomes at a concentration of 10 ng/μL. The digestion was carried out for 2 min at room temperature in 10 mM Tris-HCl, pH 7.6, 5 mM $MgCl_2$. The reaction was arrested by 100 μL of 10 mM EDTA, 0.1% SDS, 50 ng/μL proteinase K, and then the solution was incubated for 30 min at 37 °C. After phenol extraction and ethanol precipitation, the samples were separated on 8% polyacrylamide sequencing gel containing urea. The dried gel was exposed overnight on a Phosphor-Imager screen.

The protocol of Hayes and Lee (*36*) was used for the hydroxyl radical footprinting analysis.

Analytical Ultracentrifugation. Reconstituted mH2A nucleosomes were dialyzed against buffers of varying ionic strength as described in Ausió et al. (*26*). Sedimentation velocity runs were performed in a Beckman XL-A ultracentrifuge using an An-55 Al aluminum rotor. Samples were loaded in double-sector cells with aluminum filled Epon centerpieces (*37*). UV scans were taken at 260 nm and analyzed by the van Holde and Weischet (*38*) method using the XL-A Ultra Scan version 4.1 sedimentation data software (Borries Demeler, Missoula, MT).

The partial specific volume of mH2A was calculated from its amino acid analysis composition and was determined to be 0.749 cm^3/g. The partial specific volume of the mH2A containing nucleosome was calculated assuming additivity of the protein and DNA components using a partial specific volume of 0.753 cm^3/g for the rest of the histone octamer (*39*) and 0.535 cm^3/g for the DNA (*40*). The values determined in this way were 0.650 and 0.669 cm^3/g for the native and mH2A-containing nucleosome core particles, respectively.

Determination of the Hydrodynamic Parameters. It is possible to combine the known molecular masses of the nucleosome core particles (M_r = 205 600 native; M_r = 256 700 mH2A nucleosome) with their respective sedimentation coefficients to determine their conformational parameters (*41*).

Purification of Chicken Erythrocyte and HeLa Nucleosomes. Native chicken and HeLa cell mononucleosomes were prepared as described in ref *26*.

Sucrose Gradient Purification and Analysis. Reconstituted mH2A particles in 10 mM Tris-HCl (pH 7.5), 10 mM β-mercaptoethanol, 0.1 mM EDTA were loaded onto a 5−20% sucrose gradient in 25 mM NaCl, 10 mM Tris (pH 7.5), 0.1 mM EDTA and centrifuged at 134 400*g* for 19 h in a Beckman SW41 rotor at 4 °C. Gradients were collected at 1 mL/min in 0.5 mL fractions and analyzed by native gel electrophoresis.

Hydroxyapatite Chromatography of Acetylated and Nonacetylated Hela Chromatin. Purified chromatin from HeLa cell lines grown in the presence and absence of sodium butyrate were prepared (*29*) and loaded onto a hydroxyapatite column equilibrated in 0.1 mM KPO_4 (pH 6.8). Histones were fractionated by a 0−2.0 M NaCl salt gradient (*42*). The elution profile was monitored spectrophotometrically at 230 nm and was monitored by trichloroacetic acid (TCA) precipitation and SDS−PAGE analysis. TCA precipitations were performed by bringing salt solutions containing ~2 μg of protein to 20% TCA. After centrifugation at maximum speed in an Eppendorf microfuge at 4 °C, the pellet was suspended in 20% TCA and centrifuged again. The final pellet thus obtained was washed with 1.0 mL of cold 0.25 N HCl-acetone and centrifuged as described previously. The acetone pellets were dried under vacuum and resuspended in equal loading volumes of H_2O and 2X SDS-loading buffer. The elution of mH2A was monitored by Western blotting.

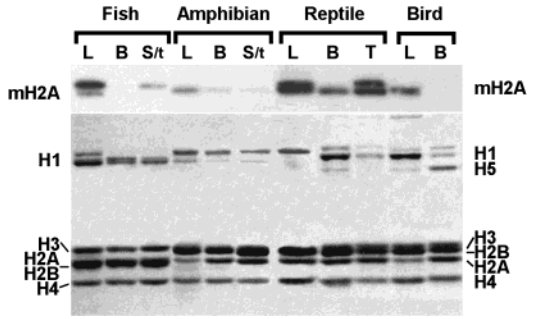

FIGURE 1: Western analysis of the distribution of macroH2A1 in different vertebrate classes. Histones were acid extracted from purified nuclei from different tissues (B: blood; L: liver; T: testes; and S: sperm) from different organisms: channel catfish, *Ictalurus ocelatus* (fish); bullfrog, *Rana caresbeiana* (amphibian); alligator, *Alligator mississipiensis* (reptile); and chicken, *Gallus domesticus* (bird). The samples were analyzed by SDS−PAGE (lower panel) and Western blot (upper panel) using mH2A1 antibody.

RESULTS

Histone mH2A Is Ubiquitously Distributed in Vertebrate Classes but Is Deficient in Terminally Differentiated Cells. Figure 1 shows the distribution of mH2A in different tissues of several representative vertebrate organisms. As it has already been reported (*43*, *44*), we could not detect the presence of this histone variant in invertebrate organisms. Within each species studied, mH2A exhibits an uneven distribution. Interestingly, the major occurrence of mH2A appears to be in liver, where with the exception of chicken (birds) the two bands corresponding to mH2A1.1 and mH2A1.2 can be observed. The mH2A abundance in liver is followed by that of testes (see Figure 1, reptile T), where the stoichiometry of mH2A1.1/mH2A1.2 appears to be highly variable. It is possible that the amount of mH2A in these two tissues is in fact the same across vertebrates as the low antigenic response observed in fish and amphibian testes is due to the large occurrence of mature spermatozoa in the samples analyzed that was absent from the reptile sample. All the erythrocytes from the species analyzed here are nucleated, and with the exception of amphibians and reptiles they do not contain significant amounts of mH2A as it has already been described (*43*). The presence of mH2A in the blood of amphibians and reptiles is probably the result of contamination by nonerythrocyte cells.

A very important observation from these results is the almost complete absence of mH2A in the sperm of the fish (catfish) and the amphibian (bullfrog) utilized for this analysis. These organisms were selected because in contrast to most vertebrates, they do not contain protamines in their mature spermatozoa but rather somatic-like histones (*45*−*47*). Gene expression is presumably nonexistent in these spermatozoa that otherwise exhibit highly condensed chro-

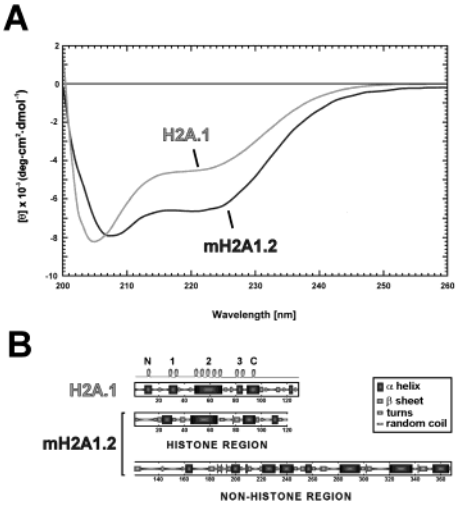

FIGURE 2: Comparative secondary structure analysis of H2A and mH2A1.2. (A) Circular dichroism spectrum of histone H2A from chicken (gray) in comparison to recombinant mH2A1.2 (black). (B) Secondary structure prediction analysis of chicken H2A.1 in comparison to rat mH2A1.2. Diverse forms of secondary structure are indicated by differential shading and box height as indicated in the inset. Positions of the α-helical domains of H2A.1 as determined from crystallographic analysis (1) are aligned above the predicted structural plots. N = amino, 1 = helix 1, 2 = helix 2, 3 = helix 3, and C = carboxyl. The NHR of mH2A1.2 is displayed underneath.

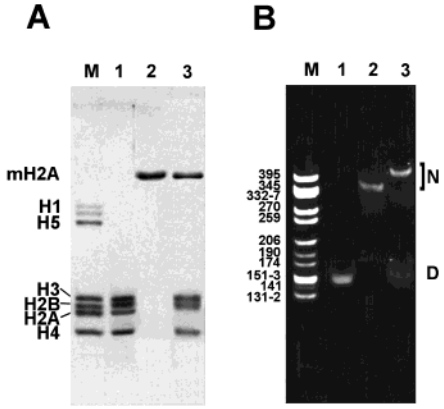

FIGURE 3: Electrophoretic characterization of mH2A1.2 containing mononucleosomes. (A) SDS−PAGE of histones from native chicken erythrocyte nucleosome core particles (lane 1), recombinant mH2A1.2 (lane 2), reconstituted mH2A1.2-containing nucleosomes, and chicken erythrocyte histones used as a marker (M). (B) 4% acrylamide native PAGE of 146 bp DNA (lane 1), native chicken erythrocyte nucleosome core particles (lane 2), reconstituted mH2A-containing nucleosomes (lane 3), and a *Cfo*I digest of pBR 322 used as a marker (M). N: nucleosome core particles and D: 146 bp DNA.

matin organization. Thus, they are analogous to the terminally differentiated erythrocytes of vertebrates. The almost complete absence of mH2A in all these terminally differentiated systems (except for the possible cell contaminations discussed previously) suggests that besides its role in X-chromosome inactivation in mammals, this histone variant most likely has a dynamic rather than passive inactivating function. Indeed, the largest occurrence of mH2A in Figure 1 happens to be in alligator testis. This is a reptile that contains a full set of protamines in the sperm as all reptiles do (*48*). The histones analyzed here came from the testis of an individual that had been captured early in the breeding season. It did not contain any mature sperm, as assessed by the complete lack of protamines, but had many cells at different premeiotic and meiotic stages (results not shown). Although the role of mH2A in meiosis has yet to be defined (*49*), its abundance in prespermiogenic testis tissue undergoing important chromatin transitions and rearrangements supports the notion that the involvement of this histone is dynamic.

C-terminal Tail of mH2A Has a Significant Amount of α-Helical Content. As a prelude to our in vitro characterization of chromatin complexes containing mH2A, we decided to look at the secondary structure of this protein to provide some insight into its physical parameters in solution. A comparative circular dichroism analysis is shown in Figure 2A. The CD spectra of both H2A and mH2A are characteristic of a predominantly α-helical conformation. By using a previously described method (*30*), the amount of α-helix can be quantitated. The amount of α-helix determined in this way was 18% for native H2A and 25% for mH2A. Assuming that the H2A-like portion of mH2A contains similar levels of α-helix (18%) in solution as its native counterpart, it is possible to calculate the α-helical composition of the NHR to be approximately 30%, which is in good agreement with the 34% value predicted from the primary structure of this domain (see Figure 2B). It is important to note that the amount of α-helix associated with histone H2A as determined from CD (results presented here in agreement with ref *50*) is lower than that observed in its histone-fold conformation (*1*, *51*) when this protein forms a complex with H2B (*52*). This suggests that the α-helical content of H2A/H2B increases upon dimer formation. Therefore, and in a similar fashion, the α-helical content of the NHR represents that of this protein region in the absence of any interaction with its putative binding partners.

Extended Conformation of mH2A-Containing Nucleosomes. The reconstitution of nucleosome core particles containing mH2A has already been reported (*15*, *16*). However, a detailed characterization of these complexes was still lacking. Figure 3 shows an electrophoretic characterization of the histones (panel A) used in the reconstitution and the DNA and particles obtained in the process (panel B). As it can be seen in Figure 3B, lanes 2 and 3, reconstituted nucleosomes consisting of two mH2A and 146 bp random sequence DNA exhibit a slightly retarded mobility as compared to native chicken erythrocyte nucleosome core particles. Upon reconstitution onto a sequence-defined DNA template, nucleosomes reconstituted with native histones or with histone octamers consisting of a mH2A complement exhibit an identical hydroxyl radical footprint (see Figure 4, lanes 4 and 5). Interestingly and in contrast to previously published results (*15*), the DNase I footprinting analysis presented here (Figure 4, lanes 2 and 3) reveals an enhanced accessibility to the enzyme near the pseudo-dyad axis of symmetry of the particle (see arrow in Figure 4) and at the sites of entry (and possibly exit) of the DNA into the nucleosome. Also, as indicated by the hydroxyl radical cleavage pattern, the trajectory of DNA around the variant octamer is consistent with control particles and random sequence nucleosomal DNA topology (~10.5 bp/turn) (*53*). Both these results are in agreement with recent observations (*16*). This suggests that histone−histone and histone−DNA interactions within the core of the nucleosome of both complexes display conformational similarity. However, a

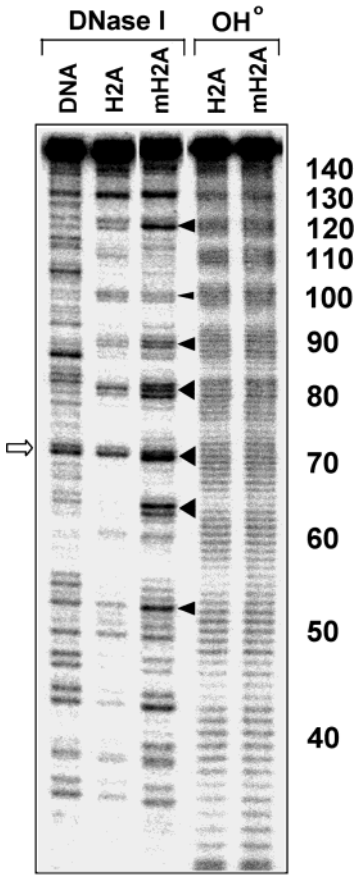

FIGURE 4: Hydroxyl radical and DNase I footprinting of mH2A nucleosomes. mH2A1.2 or conventional (H2A) nucleosomes were reconstituted with 5′-end labeled DNA and treated with either hydroxyl radical (OH•) or with DNase I and the cleavage pattern was analyzed on sequencing gels. The arrow shows the nucleosome dyad axis. The alterations in the structure of the mH2A1.2 nucleosome following DNase I digestion are designated by solid arrowheads.

unique pattern is observed for the DNase I digestion of mH2A1.2 containing mononucleosomes when compared to both naked and reconstituted nucleosomal sequence-dependent DNA. Hypersensitivity near the dyad axis of the variant complex can be attributed to the NHR extending away from this region, which allows greater accessibility of the enzyme. The difference between the two DNA footprint techniques may be explained by the size of the cleavage agent. Likely enhanced accessibility at the dyad axis and sequence-dependent topological effects are not visible following OH• treatment because the lower molecular weight of the chemical allows it to diffuse unhindered to each cleavage site.

To gain some insight into the dynamic aspects of these particles, we performed sedimentation velocity analysis of mH2A nucleosome core particles as a function of the ionic strength within physiologically relevant limits. The analysis was carried out in vitro using reconstituted nucleosome core particles (shown in Figure 3, lane 4) (see Figure 5). Reconstituted nucleosomes consisting of two mH2A molecules exhibit a rather extended conformation as indicated by the decrease in sedimentation coefficient observed under physiological ionic strength (100−150 mM NaCl) despite their 25% increase in molecular mass (see Figure 5). Furthermore, they display very similar salt-dependent stability (*41*, *54*) as that of native nucleosomes (25% DNA dissociation at 0.6 M NaCl at 20 °C) (results not shown).

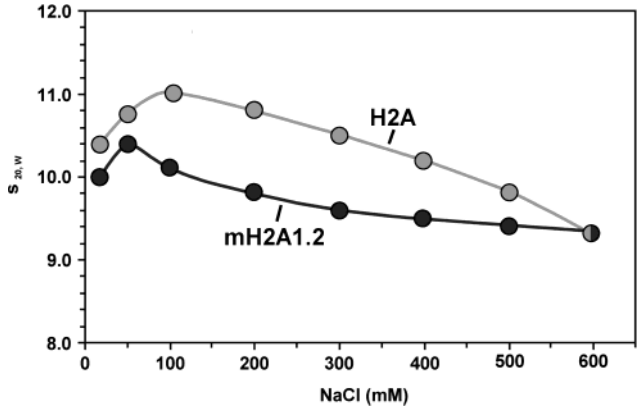

FIGURE 5: Ionic strength dependence of the sedimentation coefficient of reconstituted mH2A-containing nucleosome core particles (black) in comparison to native chicken erythrocyte nucleosome core particles (gray). The buffer used was 10 mM Tris-HCl pH 7.5, 0.1 mM EDTA, and the runs were carried out at 40 000 rpm at 20 °C.

The biophysical characterization of the mH2A nucleosome core particle shows that these particles exhibit an asymmetric conformation reflected by their lower sedimentation coefficient despite the 25% increase in mass. When the sedimentation coefficient values of the native (11.0 S) and mH2A reconstituted nucleosome core particle (10.2 S) at 100 mM NaCl (see Figure 5) are used to analyze the hydrodynamic parameters of these particles (*41*), a value of $f/f_o = 1.37$ (native) and $f/f_o = 1.64$ (mH2A) are obtained for a hydrated nucleosome core particle consisting of 0.262 g H_2O/g nucleosome as determined from the crystallographic structure (*1*). The f/f_o value for the native nucleosome is in agreement with previous data (*26*) and can be fit to a prolate ellipsoid of $a/b = 8$, whereas that of the mH2A nucleosome can be fit to a prolate ellipsoid of a semi-axes ratio $a/b = 16$.

mH2A1.2 and Chromatin. Within the context of chromatin, histone release experiments carried out with chromatin adsorbed onto hydroxyapatite (*42*, *55*) indicate that mH2A is either more strongly bound to the DNA or the rest of the histone core than its native counterpart (see Figure 6). This experiment, while it does not allow us to distinguish between these two possibilities, is in good agreement with early observations (*13*). MacroH2A elutes with a middle elution point of 1.2 M NaCl between the elution peaks of native H2A−H2B and histones H3−H4. Furthermore, as shown in the same figure, the intensity of the enhanced interaction does not appear to be dependent on the presence of high levels of acetylated histones. Therefore, the structural connection, if any, between the extent of histone acetylation and the occurrence of mH2A in inactivated chromosomal regions (*18*, *56*, *57*) remain to be elucidated.

DISCUSSION

MacroH2A is a highly specialized histone variant that appears to have had its evolutionary emergence in the vertebrates (*43*) as evidenced from its absence in invertebrate organisms. The results presented here show that mH2A exhibits a heterogeneous distribution throughout the subphylum vertebrata, and its occurrence appears to be relatively low in transcriptionally ablated, terminally differentiated cells such as nucleated erythrocytes and spermatozoa. In this regard, the use of vertebrate organisms whose sperm nuclear

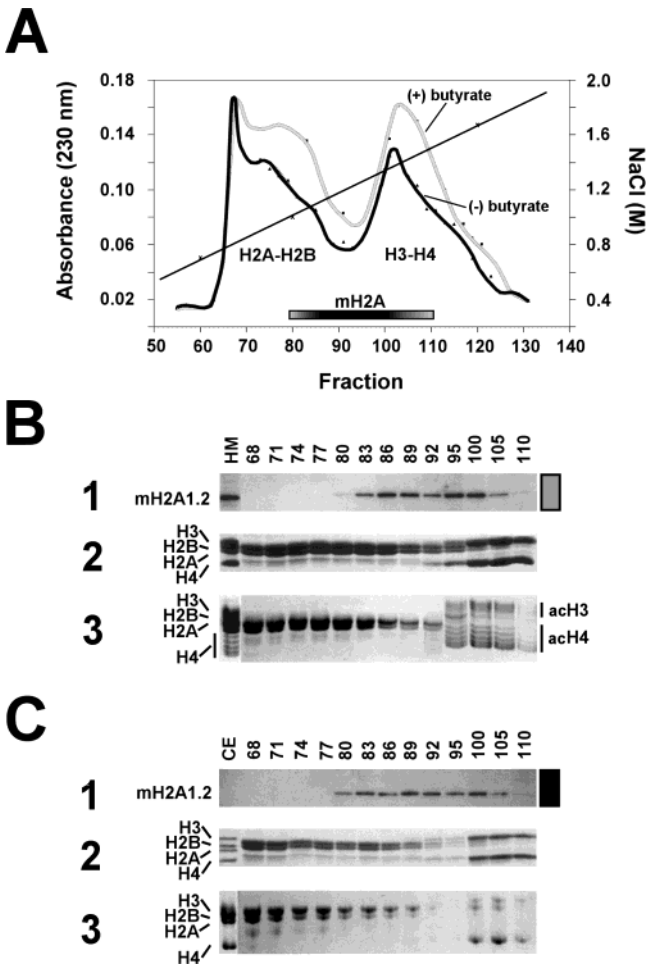

FIGURE 6: Hydroxyapatite salt-gradient fractionation of histones from chromatin obtained from HeLa cells grown in the absence or in the presence of 5 mM sodium butyrate used to raise the overall extent of histone acetylation to 10 acetyl groups per histone octamer. (A) Elution profile determined from the absorbance readings at 230 nm. The inset bar identifies the region of elution of mH2A, and the straight line indicates the NaCl gradient used for the elution of histones. (B) Western blot (1); SDS−PAGE (2); and AU−PAGE (3) analysis of different fractions obtained from the histone fractionation of chromatin from sodium butyrate-treated cells. (C) A similar analysis to that shown in panel B for chromatin obtained from untreated (control) HeLa cells. HM and CE are, respectively, total HeLa histones and chicken erythrocyte histones used as controls.

basic proteins consist of only histones, such as the catfish or the bullfrog (see Figure 1), provides a unique opportunity to study the occurrence of mH2A in vertebrate sperm. As it can be seen in Figure 1, these organisms exhibit a very low to negligible occurrence of mH2A in their sperm histone chromosomal complement. This clearly indicates that mH2A is not a significant component of vertebrate sperm as previously reported (*21*, *58*) based on the presence of mH2A in mice spermatozoa (*21*, *58*). It is important to point out here that sperm−histones are not present in all mammals, and in those in which they occur, as for instance humans, they represent only a very small fraction (<15%) of the overall chromosomal proteins (mostly composed of protamines) associated with sperm chromatin (*59*). In contrast to spermatozoa, mH2A appears to be present in early spermatogenic cells and liver. The presence in the former most likely reflects the involvement of this variant in the process of meiosis. The occurrence in liver and the absence in terminally differentiated cells are suggestive of a dynamic role of mH2A in the regulation of gene expression where it may contribute to the stabilization of transiently repressed chromatin domains. Most of the results presented here come in support of the notion of a dynamic functional role.

Is there any structural basis for such dynamic behavior that can be traced down to the basic constitutive components of the vertebrate chromosome: the nucleosome and the chromatin fiber? Despite the considerably large amount of information collected about the possible physiological relevance of mH2A (see introductory paragraphs), very little is still known about the structural consequences of the occurrence of this histone variant at the level of the nucleosome or the chromatin fiber itself. Our next studies were designed to provide insight into this characterization.

Starting from the structural analysis of the mH2A histone variant itself, the circular dichroism analysis revealed that the NHR domain contained a substantial amount of secondary structure predominantly consisting of α-helix (Figure 2). This amount is higher than that of the histone-fold domain, and it likely reflects a higher level of tertiary structure. This observation is supported by the recent crystallographic analysis carried out on an ancestral bacterial protein that displays a significant amount of sequence similarity to the NHR and is probably a homologous protein (*60*).

At the nucleosome level, we carried out in vitro analysis. To this end, we used reconstituted nucleosome core particles and sedimentation velocity for their characterization (Figures 3−5). Although it is difficult to fit the structure of the nucleosome to hydrodynamic models (the structure of the nucleosome core particle would correspond to a predicted solid oblate ellipsoid of $a/b = 2$), the result nevertheless indicates that the mH2A particle is at least twice as asymmetrical as the native nucleosome core particle (see Figure 7 A for a model). Furthermore, the DNA in the vicinity of the dyad axis and around the entry and exit sites is more exposed to DNase I, suggesting a more extended organization in this region of the C-terminal tail of mH2A as compared to H2A (Figure 7A). However, the overall conformation is significantly compacted as this domain would span about 700 Å in a completely linear conformation (see Figure 7B). The folded structure of the NHR domain of mH2A implied by our hydrodynamic studies is consistent with the recent crystallographic data from the bacterial NHR-like protein (*60*).

At the level of the chromatin fiber, high levels of histone acetylation did not alter the enhanced interaction of mH2A1.2 within the nucleosome (Figure 6). The full significance of mH2A deposition within specialized nucleosomes is poorly understood. On the basis of its enrichment in heterochromatinized sex chromatin (*18*) and repression of transcription initiation (*24*), it is likely that this histone variant is important for lowering the permissibility of gene expression. Indeed, a stabilizing structural role independent of histone acetylation levels is in agreement with the observation that the histone region of mH2A1.2 is more resistant to chromatin remodeling in situ (*16*).

It is possible that mH2A has acquired different roles in the course of vertebrate evolution. While initially designed as a repressive histone variant involved in the regulation of transcription through mechanisms that involve alteration of chromatin remodeling and transcription factor binding ac-

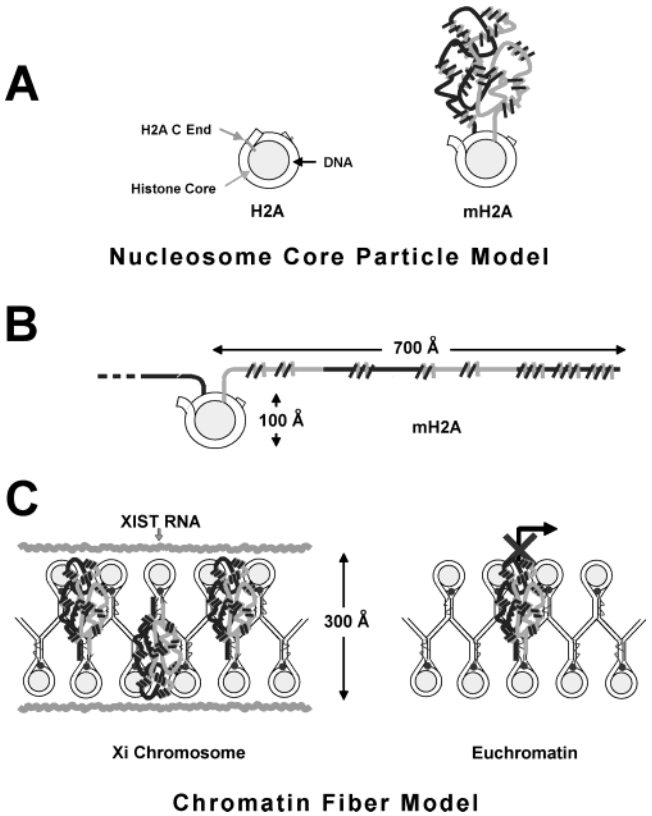

FIGURE 7: Schematic representation of the mH2A nucleosome. (A) As assessed from its hydrodynamic parameters. (B) For comparative purposes, a conformation where the C-terminal NHR adopts a completely extended structure is shown. The protein backbone span was calculated using a distance between adjacent amino acids of 3.63 Å in a fully extended chain and 1.50 Å in a helical conformation (*62*) and the α-helical content experimentally determined in this paper. (C) A model for incorporation of mH2A nucleosomes within chromatin. Various possibilities for the functionally relevant structure of the nucleosome model shown in panel A include (1) interactions with *Xist* RNA in during sex-linked heterochromatinization and (2) participation in the dynamic inactivation events.

cessibility (*16*) (see Figure 7C), mammals appear to have taken further advantage of this variant's repressive role for the purpose of X-chromosome inactivation by creating chromatin domains that facilitate interactions with *Xist* RNA (*43*, *56*, *61*) (see Figure 7C). Further experiments are required to characterize the bifunctional properties of mH2A containing chromatin in both the Xi and the active regions of the genome.

ACKNOWLEDGMENT

We wish to thank John R. Pehrson for his generous contribution of mH2A1 antibody and recombinant protein expression plasmid.

REFERENCES

1. Luger, K., Mader, A. W., Richmond, R. K., Sargent, D. F., and Richmond, T. J. (1997) Crystal structure of the nucleosome core particle at 2.8 Å resolution, *Nature 389*, 251−260.
2. Knezetic, J. A., and Luse, D. S. (1986) The presence of nucleosomes on a DNA template prevents initiation by RNA polymerase II in vitro, *Cell 45*, 95−104.
3. Matsui, T. (1987) Transcription of adenovirus 2 major late and peptide IX genes under conditions of in vitro nucleosome assembly, *Mol. Cell. Biol. 7*, 1401−1408.
4. Wilkins, R. J., and Hart, R. W. (1974) Preferential DNA repair in human cells, *Nature 247*, 35−36.
5. Wang, Z. G., Wu, X. H., and Friedberg, E. C. (1991) Nucleotide excision repair of DNA by human cell extracts is suppressed in reconstituted nucleosomes, *J. Biol. Chem. 266*, 22472−22478.
6. Sugasawa, K., Masutani, C., and Hanaoka, F. (1993) Cell-free repair of UV-damaged simian virus 40 chromosomes in human cell extracts. I. Development of a cell-free system detecting excision repair of UV-irradiated SV40 chromosomes, *J. Biol. Chem. 268*, 9098−9104.
7. Strahl, B. D., and Allis, C. D. (2000) The language of covalent histone modifications, *Nature 403*, 41−45.
8. Turner, B. M. (2000) Histone acetylation and an epigenetic code, *Bioessays 22*, 836−845.
9. Ausió, J., Abbott, D. W., Wang, X., and Moore, S. C. (2001) Histone variants and histone modifications: a structural perspective, *Biochem. Cell Biol. 79*, 693−708.
10. Ausió, J., and Abbott, D. W. (2002) The many tales of a tail: carboxyl-terminal tail heterogeneity specializes histone H2A variants for defined chromatin function, *Biochemistry 41*, 5945−5949.
11. Wolffe, A. P., and Dimitrov, S. (1993) Histone-modulated gene activity: developmental implications, *Crit. Rev. Eukaryot. Gene Expr. 3*, 167−191.
12. Alvelo-Ceron, D., Niu, L., and Collart, D. G. (2000) Growth regulation of human variant histone genes and acetylation of the encoded proteins, *Mol. Biol. Rep. 27*, 61−71.
13. Pehrson, J. R., and Fried, V. A. (1992) MacroH2A, a core histone containing a large nonhistone region, *Science 257*, 1398−1400.
14. Chadwick, B. P., and Willard, H. F. (2002) Cell cycle-dependent localization of macroH2A in chromatin of the inactive X chromosome, *J. Cell Biol. 157*, 1113−1123.
15. Changolkar, L. N., and Pehrson, J. R. (2002) Reconstitution of nucleosomes with histone macroH2A1.2, *Biochemistry 41*, 179−184.
16. Angelov, D., Molla, A., Perche, P. Y., Hans, F., Cote, J., Khochbin, S., Bouvet, P., and Dimitrov, S. (2003) The histone variant macroH2A interferes with transcription factor binding and SWI/SNF nucleosome remodeling, *Mol. Cell 11*, 1033−1041.
17. Pehrson, J. R., Costanzi, C., and Dharia, C. (1997) Developmental and tissue expression patterns of histone macroH2A1 subtypes, *J. Cell. Biochem. 65*, 107−113.
18. Costanzi, C., and Pehrson, J. R. (1998) Histone macroH2A1 is concentrated in the inactive X chromosome of female mammals, *Nature 393*, 599−601.
19. Costanzi, C., Stein, P., Worrad, D. M., Schultz, R. M., and Pehrson, J. R. (2000) Histone macroH2A1 is concentrated in the inactive X chromosome of female preimplantation mouse embryos, *Development 127*, 2283−2289.
20. Chadwick, B. P., and Willard, H. F. (2001) A novel chromatin protein, distantly related to histone H2A, is largely excluded from the inactive X chromosome, *J. Cell Biol. 152*, 375−384.
21. Hoyer Fender, S., Costanzi, C., and Pehrson, J. R. (2000) Histone macroH2A1.2 is concentrated in the XY-body by the early pachytene stage of spermatogenesis, *Exp. Cell Res. 258*, 254−260.
22. Richler, C., Dhara, S. K., and Wahrman, J. (2000) Histone macroH2A1.2 is concentrated in the XY compartment of mammalian male meiotic nuclei, *Cytogenet. Cell Genet. 89*, 118−120.
23. Rasmussen, T. P., Huang, T., Mastrangelo, M. A., Loring, J., Panning, B., and Jaenisch, R. (1999) Messenger RNAs encoding mouse histone macroH2A1 isoforms are expressed at similar levels in male and female cells and result from alternative splicing, *Nucleic Acids Res. 27*, 3685−3689.
24. Perche, P. Y., Vourc'h, C., Konecny, L., Souchier, C., Robert-Nicoud, M., Dimitrov, S., and Khochbin, S. (2000) Higher concentrations of histone macroH2A in the Barr body are correlated with higher nucleosome density, *Curr. Biol. 10*, 1531−1534.
25. Turner, J. M., Burgoyne, P. S., and Singh, P. B. (2001) M31 and macroH2A1.2 colocalise at the pseudoautosomal region during mouse meiosis, *J. Cell Sci. 114*, 3367−3375.
26. Ausió, J., Dong, F., and van Holde, K. E. (1989) Use of selectively trypsinized nucleosome core particles to analyze the role of the histone "tails" in the stabilization of the nucleosome, *J. Mol. Biol. 206*, 451−463.
27. Wang, X., and Ausió, J. (2001) Histones are the major chromosomal protein components of the sperm of the nemerteans

Cerebratulus californiensis and *Cerebratulus lacteus*, *J. Exp. Zoo. 290*, 431−436.
28. Sambrook, J., Fritsch, E. F., and Maniatis, T. (1989) *Molecular Cloning, A Laboratory Manual*, 2nd ed. Cold Spring Harbor Laboratory Press, Cold Spring Harbor, NY.
29. Ausió, J., and van Holde, K. E. (1986) Histone hyperacetylation: its effects on nucleosome conformation and stability, *Biochemistry 25*, 1421−1428.
30. Wang, X., Moore, S. C., Laszckzak, M., and Ausió, J. (2000) Acetylation increases the α-helical content of the histone tails of the nucleosome, *J. Biol. Chem. 275*, 35013−35020.
31. Geourjon, C., and Deleage, G. (1994) SOPM: a self-optimized method for protein secondary structure prediction, *Protein Eng. 7*, 157−164.
32. Abbott, D. W., Ivanova, V. S., Wang, X., Bonner, W. M., and Ausió, J. (2001) Characterization of the stability and folding of H2A.Z chromatin particles: implications for transcriptional activation, *J. Biol. Chem. 276*, 41945−41949.
33. Laemmli, U. K. (1970) Cleavage of structural proteins during the assembly of the head of bacteriophage T4, *Nature 227*, 680−685.
34. Ausió, J., and Moore, S. C. (1998) Reconstitution of chromatin complexes from high-performance liquid chromatography-purified histones, *Methods 15*, 333−342.
35. Yager, T. D., and van Holde, K. E. (1984) Dynamics and equilibria of nucleosomes at elevated ionic strength, *J. Biol. Chem. 259*, 4212−4222.
36. Hayes, J. J., and Lee, K. M. (1997) In vitro reconstitution and analysis of mononucleosomes containing defined DNAs and proteins, *Methods 12*, 2−9.
37. Garcia Ramirez, M., Dong, F., and Ausió, J. (1992) Role of the histone "tails" in the folding of oligonucleosomes depleted of histone H1, *J. Biol. Chem. 267*, 19587−19595.
38. van Holde, K. E., and Weischet, W. O. (1978) Boundary analysis of sedimentation velocity experiments with monodisperse and paucidisperse solutes, *Biopolymers 17*, 1387−1403.
39. Eickbush, T. H., and Moudrianakis, E. N. (1978) The histone core complex: an octamer assembled by two sets of protein−protein interactions, *Biochemistry 17*, 4955−4964.
40. Eisenberg, H. (1976) *Biological Macromolecules and Polyelectrolytes in Solution*, Clarendon Press, Oxford.
41. Ausió, J. (2000) Analytical ultracentrifugation and the characterization of chromatin structure, *Biophys. Chem. 86*, 141−153.
42. Simon, R. H., and Felsenfeld, G. (1979) A new procedure for purifying histone pairs H2A + H2B and H3 + H4 from chromatin using hydroxylapatite, *Nucleic Acids Res. 6*, 689−696.
43. Pehrson, J. R., and Fuji, R. N. (1998) Evolutionary conservation of histone macroH2A subtypes and domains, *Nucleic Acids Res. 26*, 2837−2842.
44. Costanzi, C., and Pehrson, J. R. (2001) MACROH2A2, a new member of the MARCOH2A core histone family, *J. Biol Chem. 276*, 21776−21784.
45. Itoh, T., Ausió, J., and Katagiri, C. (1997) Histone H1 variants as sperm-specific nuclear proteins of *Rana catesbeiana* and their role in maintaining a unique condensed state of sperm chromatin, *Mol. Reprod. Dev. 47*, 181−190.
46. Kasinsky, H. E. (1989) *Specificity and distribution of sperm basic proteins*, CRC Press Inc., Boca Raton, FL.
47. Saperas, N., Ausió, J., Lloris, D., and Chiva, M. (1994) On the evolution of protamines in bony fish: alternatives to the "retroviral horizontal transmission" hypothesis, *J. Mol. Evol. 39*, 282−295.
48. Hunt, J. G., Kasinsky, H. E., Elsey, R. M., Wright, C. L., Rice, P., Bell, J. E., Sharp, D. J., Kiss, A. J., Hunt, D. F., Arnott, D. P. et al. (1996) Protamines of reptiles, *J. Biol. Chem. 271*, 23547−23557.
49. Lewis, J. D., Abbott, D. W., and Ausio, J. (2003) A haploid affair: core histone transitions during spermatogenesis, *Biochem. Cell Biol. 81*, 8077−8091.
50. D'Anna, J. A., and Isenberg, I. (1974) Interactions of histone LAK (f2a2) with histones KAS (f2b) and GRK (f2a1), *Biochemistry 13*, 2098−2104.
51. Arents, G., Burlingame, R. W., Wang, B. C., Love, W. E., and Moudrianakis, E. N. (1991) The nucleosomal core histone octamer at 3.1 Å resolution: a tripartite protein assembly and a left-handed superhelix, *Proc. Natl. Acad. Sci. U.S.A. 88*, 10148−10152.
52. Karantza, V., Freire, E., and Moudrianakis, E. N. (2001) Thermodynamic studies of the core histones: stability of the octamer subunits is not altered by removal of their terminal domains, *Biochemistry 40*, 13114−13123.
53. Bauer, W. R., Hayes, J. J., White, J. H., and Wolffe, A. P. (1994) Nucleosome structural changes due to acetylation, *J. Mol. Biol. 236*, 685−690.
54. Ausió, J., Seger, D., and Eisenberg, H. (1984) Nucleosome core particle stability and conformational change. Effect of temperature, particle, and NaCl concentrations and cross-linking of histone H3 sulfhydryl groups, *J. Mol. Biol. 176*, 77−104.
55. Li, W., Nagaraja, S., Delcuve, G. P., Hendzel, M. J., and Davie, J. R. (1993) Effects of histone acetylation, ubiquitination, and variants on nucleosome stability, *Biochem. J. 296*, 737−744.
56. Gilbert, S. L., Pehrson, J. R., and Sharp, P. A. (2000) XIST RNA associates with specific regions of the inactive X chromatin, *J. Biol. Chem. 275*, 36491−36494.
57. Mermoud, J. E., Popova, B., Peters, A. H., Jenuwein, T., and Brockdorff, N. (2002) Histone H3 lysine 9 methylation occurs rapidly at the onset of random X chromosome inactivation, *Curr. Biol. 12*, 247−251.
58. Pittoggi, C., Renzi, L., Zaccagnini, G., Cimini, D., Degrassi, F., Giordano, R., Magnano, A. R., Lorenzini, R., Lavia, P., and Spadafora, C. (1999) A fraction of mouse sperm chromatin is organized in nucleosomal hypersensitive domains enriched in retroposon DNA, *J. Cell Sci. 112*, 3537−3548.
59. Gatewood, J. M., Cook, G. R., Balhorn, R., Schmid, C. W., and Bradbury, E. M. (1990) Isolation of four core histones from human sperm chromatin representing a minor subset of somatic histones, *J. Biol. Chem. 265*, 20662−20666.
60. Allen, M. D., Buckle, A. M., Cordell, S. C., Lowe, J., and Bycroft, M. (2003) The crystal structure of AF1521 a protein from *Archaeoglobus fulgidus* with homology to the nonhistone domain of macroH2A, *J. Mol. Biol. 330*, 503−511.
61. Csankovszki, G., Panning, B., Bates, B., Pehrson, J. R., and Jaenisch, R. (1999) Conditional deletion of Xist disrupts histone macroH2A localization but not maintenance of X inactivation, *Nat. Genet. 22*, 323−324.
62. Creighton, T. E. (1996) *Proteins*, 2nd ed., W. H. Freeman and Co., New York.

BI035859I